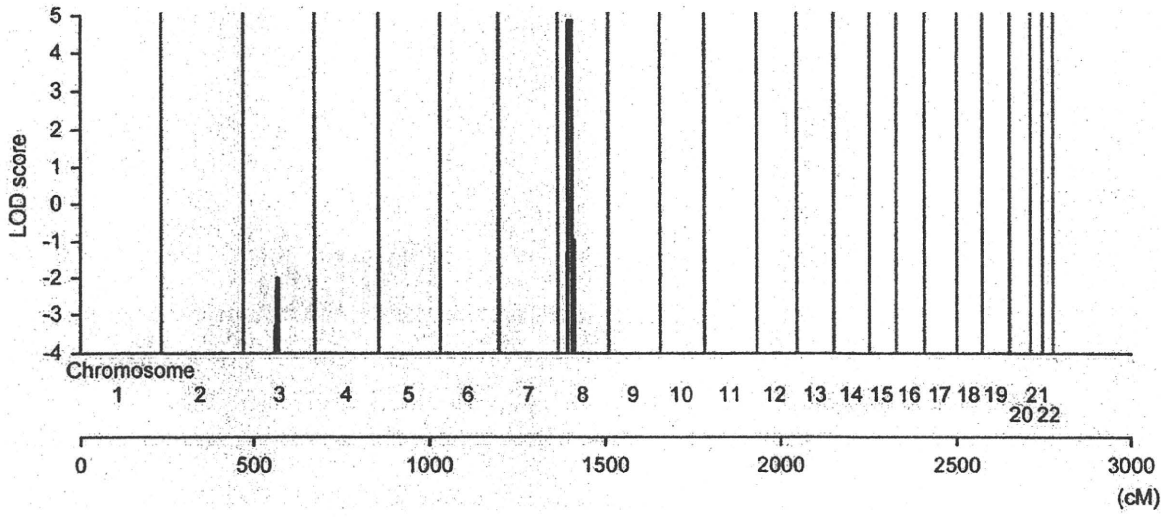

Figure S2. Parametric Linkage Analysis of Families 1 and 2 Using Affected Individuals Only

Cumulative maximum multipoint parametric lod score is shown. Horizontal axis represents the cumulative map position (cM) on the chromosomes 1-22. Family 1 was divided into 2 branches for calculation of LOD score as indicated.

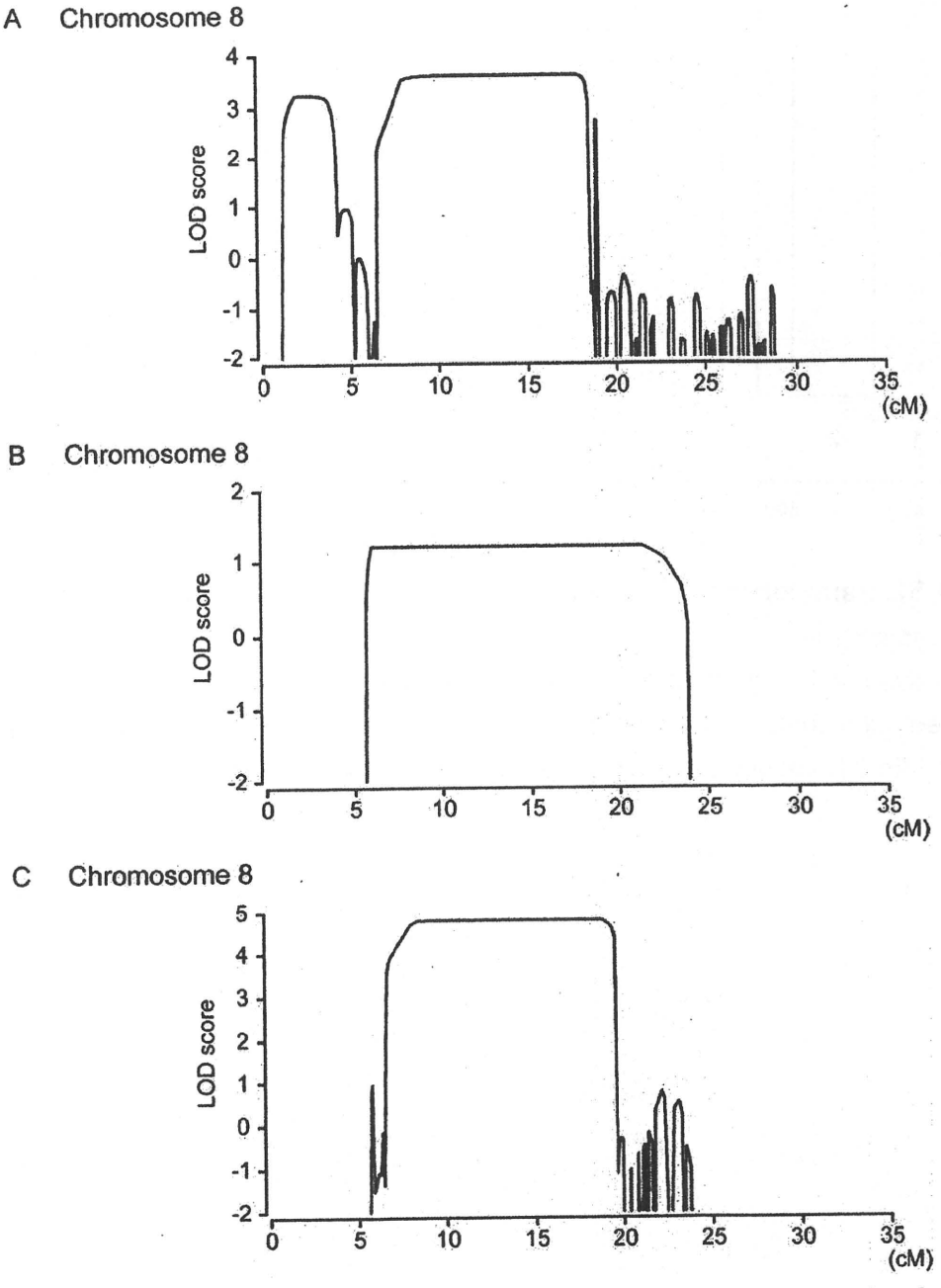

Figure S3. Parametric Linkage Analysis (Affected Individuals Only) at Loci on the Short Arm of Chromosome 8

Only the phenotypes of affected individuals are explicitly indicated in the analysis, while those of other individuals are indicated as "unknown". Maximum multipoint parametric lod scores for Families 1 (A) and 2 (B), and cumulative lod score for Families 1 and 2 (C) are shown. Since the family structure of Family 1 was too large for calculation, the family structure was divided into 2 branches for calculation of LOD score as indicated. Horizontal axis is the map position (cM) on the short arm of chromosome 8.

Table S1. Natural Variant in RP1L1 Sequence in OMD Families

cDNA change	Amino acid change	dbSNP.ID	Number of observed mutations/affected subjects (frequency)	Number of observed mutations/unaffected subjects (frequency)
c.518 G>C	E97Q	ss252841181	0/ 12 (0.00)	1/ 21 (0.05)
c.730 A>G	T167 synonymous	rs79329877	2/ 10 (0.20)	1/ 20 (0.05)
c.894 A>C	H222P	rs4388421	5/ 12 (0.42)	5/ 21 (0.24)
c.1769 G>A	G514S	rs74990397	3/ 12 (0.25)	3/ 21 (0.14)
c.2020 C>T	G597 synonymous	rs6996950	12/ 12 (1.00)	21/ 21 (1.00)
c.2497 C>T	N756 synonymous	rs57819090	4/ 12 (0.33)	3/ 21 (0.14)
c.2604 T>C	L792P	rs35602868	3/ 12 (0.25)	3/ 21 (0.14)
c.2807 C>T	R860W	rs62490856	3/ 12 (0.25)	2/ 21 (0.10)
c.3665 C>T	R1146W	rs4840502	12/ 12 (1.00)	21/ 21 (1.00)
c.4630 G>T	R1467S	rs4840498	12/ 12 (1.00)	21/ 21 (1.00)
c.4677 C>T	A1483V	rs62490855	1/ 12 (0.08)	0/ 21 (0.00)
c.4713 C>G	P1495R	rs4841399	10/ 12 (0.83)	21/ 21 (1.00)
c.5182 G>A	A1659 synonymous	ss252841182	1/ 12 (0.08)	3/ 21 (0.14)
c.5355 C>T	A1709V	rs13267180	3/ 12 (0.25)	3/ 21 (0.14)
c.5895 A>T	D1889V	rs28446662	9/ 12 (0.75)	18/ 19 (0.95)
c.6647 G>A	E2140K	rs72494282	5/ 12 (0.42)	5/ 21 (0.24)
c.6740 G>A	E2171K	rs4354268	2/ 12 (0.17)	1/ 21 (0.05)
c.6952 A>G	S2241 synonymous	rs56382513	11/ 12 (0.92)	20/ 21 (0.95)
c.7082 G>A	G2285R	rs55642448	11/ 12 (0.92)	21/ 21 (1.00)

Nucleotides and amino acid are numbered as in GenBank accesssion number NM_178857 and NP_849188.4, respectively. Sequencing of the CDS excluding repeat site (approximately 3960 to 4320 and 5980 to 6480; NM_178857) of RP1L1 in OMD family members.

Human Molecular Genetics, 2010, Vol. 19, No. 13 **2606–2615**
doi:10.1093/hmg/ddq146
Advance Access published on April 13, 2010

Overexpression of optineurin E50K disrupts Rab8 interaction and leads to a progressive retinal degeneration in mice

Zai-Long Chi[1,†], Masakazu Akahori[1,†], Minoru Obazawa[1], Masayoshi Minami[1], Toru Noda[1], Naoki Nakaya[2], Stanislav Tomarev[2], Kazuhide Kawase[3], Tetsuya Yamamoto[3], Setsuko Noda[4], Masaki Sasaoka[5], Atsushi Shimazaki[5], Yuichiro Takada[1] and Takeshi Iwata[1,*]

[1]National Institute of Sensory Organs, National Hospital Organization Tokyo Medical Center, 2-5-1 Higashigaoka, Meguro-ku, Tokyo 152-8902, Japan, [2]National Eye Institute, National Institutes of Health, 5635 Fishers Lane, Room 1124, Rockville, MD 20852, USA, [3]Department of Ophthalmology, Gifu University Graduate School of Medicine, 1-1 Yanagido, Gifu 501-1194, Japan, [4]Department of Nursing, Tokai University School of Health Sciences, Boseidai, Isehara, Kanagawa Prefecture 259-1193, Japan and [5]Research & Development Center, Santen Pharmaceutical Co., Ltd, 8916-16, Takayama-cho, Ikoma, Nara Prefecture 630-0101, Japan

Received March 16, 2010; Revised and Accepted April 12, 2010

Glaucoma is one of the leading causes of bilateral blindness affecting nearly 8 million people worldwide. Glaucoma is characterized by a progressive loss of retinal ganglion cells (RGCs) and is often associated with elevated intraocular pressure (IOP). However, patients with normal tension glaucoma (NTG), a subtype of primary open-angle glaucoma (POAG), develop the disease without IOP elevation. The molecular pathways leading to the pathology of NTG and POAG are still unclear. Here, we describe the phenotypic characteristics of transgenic mice overexpressing wild-type (Wt) or mutated optineurin (Optn). Mutations E50K, H486R and Optn with a deletion of the first (amino acids 153–174) or second (amino acids 426–461) leucine zipper were used for overexpression. After 16 months, histological abnormalities were exclusively observed in the retina of E50K mutant mice with loss of RGCs and connecting synapses in the peripheral retina leading to a thinning of the nerve fiber layer at the optic nerve head at normal IOP. E50K mice also showed massive apoptosis and degeneration of entire retina, leading to approximately a 28% reduction of the retina thickness. At the molecular level, introduction of the E50K mutation disrupts the interaction between Optn and Rab8 GTPase, a protein involved in the regulation of vesicle transport from Golgi to plasma membrane. Wt Optn and an active GTP-bound form of Rab8 complex were localized at the Golgi complex. These data suggest that alternation of the Optn sequence can initiate significant retinal degeneration in mice.

INTRODUCTION

Glaucoma is characterized by progressive loss of retinal ganglion cells (RGCs), degeneration of axons in the optic nerve and visual field defects. Primary open-angle glaucoma (POAG) is one of the major causes of irreversible blindness leading to vision loss in about 4.5 million people and accounting for 12% of global blindness (1,2). POAG is often associated with elevated intraocular pressure (IOP), which is one of main risk factors in glaucoma. However, degenerative changes in the RGC and the optic nerve head leading to progressive visual field loss may occur even in the absence of elevated IOP in a subtype of POAG called normal tension glaucoma (NTG). A recent epidemiological study in Tajimi,

*To whom correspondence should be addressed. Tel/Fax: +81 334111026; Email: iwatatakeshi@kankakuki.go.jp
†The first two authors contributed equally to this work.

Japan, demonstrated that >90% of POAG cases were diagnosed as NTG (3).

At least 24 different genetic loci have been linked to various forms of glaucoma, and four glaucoma-associated genes, *myocilin*, *cytochrome P4501B1*, *OPTN* and *WD repeat domain 36* (*WDR36*) have been previously identified (4–7). A significantly higher frequency of *OPTN* sequence alternations in glaucoma subjects compared with controls supports the contribution of this gene to the development of glaucoma (8–10). In one original report, >16.7% of NTG families had mutations in the *OPTN* gene (6), and a number of disease-causing amino acid substitutions including E50K, H486R and R545Q have been confirmed by others (8–10). The substitution of glutamic acid by lysine at amino acid 50 (E50K) is exclusively associated with familial and sporadic forms of NTG (6,8,11). We also identified E50K mutation in an NTG family in Japan (Supplementary Material 1). Several lines of evidence support E50K mutation could play a critical role for the severity of phenotype and pathology of glaucoma. Clinical study revealed that an NTG phenotype is more severe in subjects with the E50K mutation than in a control group of subjects with NTG but without this mutation, supporting a critical role for this mutation (8,12). *In vitro* cell biological study demonstrated that transfection of E50K-mutated optineurin (Optn) caused cell death of rat RGC cell line, RGC5 (13).

OPTN corresponds to the *GLC1E* locus for adult-onset POAG and is located in the 10p14 region. The *OPTN* gene contains 3 non-coding exons followed by 13 exons encoding a 577 amino acid protein. Almost all of the reported disease-causing mutations correspond to positions that are evolutionarily conserved between the mouse, monkey and human. OPTN is ubiquitously expressed in all tissues and interacts with number of proteins including huntingtin (14), transcription factor IIIA (15), Rab8 (16,17), myosin VI (18), FOS (19), ring finger protein 11 (20) and metabotrophic glutamate receptor 1-a (21), suggesting multiple cellular functions. Recent studies have shown that the *OPTN* promoter is induced by TNF-α (22). OPTN may function as an adaptor which regulates the assembly of TAX1BP1 and the post-translationally modified form of Tax1, leading to a sustained NF-κB activation (23).

The molecular pathways leading to glaucoma from a single gene mutation still remain unclear mainly due to (i) insufficiency of clinical and genetic information from glaucoma patients, (ii) difficulty in obtaining clinical material, such as optic nerve tissues, from patients and (iii) lack of animal models with particular gene mutations. Recently, it has been reported that glutamate transporter-deficient mice exhibit an NTG-like phenotype (24). However, to this date, no animal models have been produced based on the gene mutation found in NTG patients.

In this paper, we developed five variants of *Optn* overexpressing mice including the wild-type (Wt), E50K and H486R point mutants, and mutants with a deletion of the first or second leucine zipper. We used histopathology to investigate changes in the optic nerve and retina of each mutant. Using a modified protein fragment complementation method, we also investigated the effects of the E50K mutation on the interaction with OPTN-interacting protein Rab8, which controls the vesicle transport.

RESULTS

Construction of mouse Optn mutants and characterization of expression

Five mouse Optn variants were overexpressed under the CMV early enhancer/chicken beta-actin (CAG) promoter in transgenic mice. These variants included Wt Optn, the E50K and H489R mutants which are mouse equivalents of the human glaucoma-causing mutations E50K and H486R, respectively, and mutants with deletion of the first (1st LZ del) or second (2nd LZ del) Optn leucine zipper domain. All transgenic mice were born at normal Mendelian ratios, weighed the same as non-transgenic littermates and appeared normal up to 16 months of age. The mutant HA-tagged proteins were ubiquitously expressed in the entire retina (Fig. 1B). The copy numbers for each mutant cDNA construct were approximately 12 to 14 per mouse as determined by TaqMan real-time PCR assay (data not shown).

Comparison of histological changes in the eye of Wt and mutant Optn transgenic mice

Loss of RGCs and cupping of the optic disc are the defining histological features of the retina of patients with POAG and NTG. Therefore, we examined the eyes of aged Wt, E50K, H489R, 1st LZ del and 2nd LZ del mice using histology and immunohistochemistry. Cornea, lens and anterior segment of Wt and transgenic mice were histologically normal even in 16-month-old mice. For statistical analysis, measurements of retinal thickness were made at the peripheral retina ~1.0–1.2 mm from the optic nerve head. Remarkably, we found significant phenotypical changes in five independent transgenic mouse lines expressing the E50K mutant (Fig. 2A). The retinal thickness of E50K mice was significantly reduced compared with Wt mice at 16 months of age ($^*P < 0.05$) (Fig. 2B), but a reduction of the retinal thickness was observed as early as 12 months of age (Fig. 2C). Owing to the loss of RGCs and their axons in the peripheral retina, β-III tubulin-stained nerve fiber layer was relatively thinner at the optic nerve head of E50K mice compared with Wt mice (Fig. 2D). The anti-SMI32 immunostaining of the whole-mounted retina demonstrated loss of large RGCs in the peripheral retina (Fig. 2D). Progressive, non-specific loss of RGCs in E50K mice was shown by counting NeuN-stained cells in the entire retina sections (Fig. 2D).

To determine which retinal cell types are vulnerable to the E50K mutation, we performed immunohistochemical analysis using retinal cell-specific markers. Immunostaining with calretinin antibodies was used to visualize synapses of RGCs and amacrine cells in the inner plexiform layer of 16-month-old Wt and E50K mice (Fig. 3A). Although there was no difference in the immunolabeling pattern of synapses in the central retina of Wt and E50K mice (Box C**), a significant degeneration of synapses was observed in the peripheral retina of E50K mice versus Wt mice (Box P**). Immunolabeling of the flat mount retina using antibodies against choline acetyltransferase (ChAT, cholinergic amacrine) revealed areas of amacrine cell loss in the peripheral retina (Box P**) (Fig. 3B, arrow). Loss and/or changes of another type of amacrine cells and rod bipolar cells in the peripheral retina of

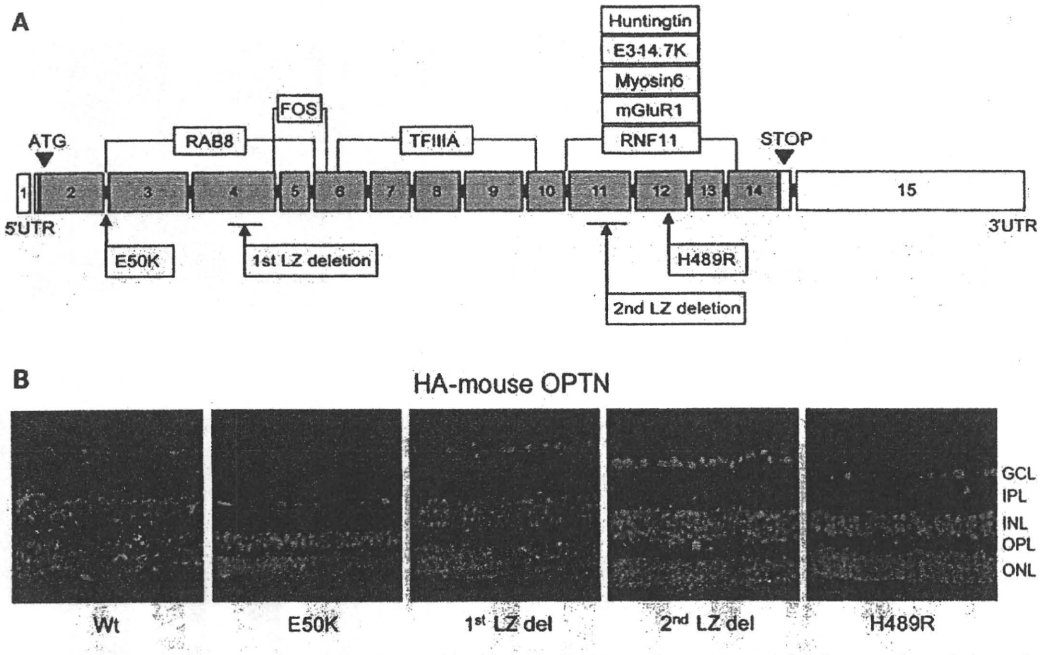

Figure 1. (**A**) Schematic diagram of the mouse Optn constructs used in this study. Positions of mutations and deletions are shown in lower boxes. Predicted binding sites of Optn-interacting proteins are shown in upper boxes. (**B**) Expression of Optn mutants in the retina of transgenic mice. Sections were immunostained with anti-HA antibody. Scale bar: 20 μm.

E50K mice versus Wt were detected by staining with antibodies against tyrosine hydroxylase (red, doperminergic amacrine cell) and PKC α (green, rod bipolar cell) (Fig. 3C, Box P**). The outer plexiform layer (OPL) and outer nuclear layer (ONL) were also affected in E50K mice. In the OPL, expression of synaptophysin, synaptic vesicle marker at the photoreceptor synaptic terminal, was reduced in E50K mice compared with Wt mice (Fig. 4), whereas rhodopsin-labeled outer segments were shorter in E50K mutant than in Wt mice.

Apoptosis assay by single-stranded DNA immunohistochemistry

RGC death by apoptosis is one of the typical features of glaucoma pathogenesis. Immunostaining with antibodies against single-stranded DNA (ssDNA), a marker of apoptosis-associated DNA damage, was used to detect apoptotic changes in the retina of E50K mice. ssDNA-positive (apoptotic) cells were detected not only in the RGCL (Fig. 4A, Arrow) but also in the INL and ONL. At the peripheral retina, significant increase of apoptotic cell number in all retinal layers was observed in E50K mice at 16 months of age (Fig. 4B) compared with age-matched Wt mice ($^{**}P < 0.01$).

IOP of Wt and mutant *Optn* transgenic mice

IOP measurement is a necessary and important step to determine whether retinal degeneration in our transgenic mice is associated with the elevation of IOP or it is IOP independent. IOP was measured using an impact-rebound tonometer and an optical interferometry tonometer. The average IOP reading from both devices gave similar IOP for mutant and Wt mice in the normal range of 15 ± 1 mmHg for all examined ages (Fig. 5). These results demonstrated that pathological features of E50K mice are not due to changes in IOP.

E50k mutation disrupts OPTN–Rab8 direct protein interaction

Protein–protein interaction of OPTN and Rab8 was analyzed after transfection of RGC5 or COS1 cells with constructs encoding OPTN (Wt, E50K), Rab8 [Wt, T22N (inactive GDP form) and Q67L (active GTP form)] tagged with fluorescent labels (Fig. 6A). We observed >4-fold decrease in the interaction between OPTN Wt and the active form (Q67L) versus the inactive form (T22N) of Rab8. However, E50K did not interact with either form of Rab8 in RGC5 cells (Fig. 6B). Interaction of Wt OPTN and the active form Rab8 was further supported by co-localization of the complex with a specific Golgi marker, GM130, in COS1 cells (Fig. 6C).

DISCUSSION

In the present study, we produced and characterized the phenotype of five different transgenic *Optn* mice lines including lines with overexpression of two *OPTN* mutations identified in glaucoma patients. Among the 15 *OPTN* mutations previously identified (P16A, H26D, E50K, K66R, E92V, E103D, 2 bp insertion between amino acids 127–128, V161M, H228Y, A336G, A377T, I407T, A466S, H486R and R545Q), we selected two mutations E50K and H486R, which has been confirmed by several groups to be associated with severe NTG and/or juvenile open-angle glaucoma

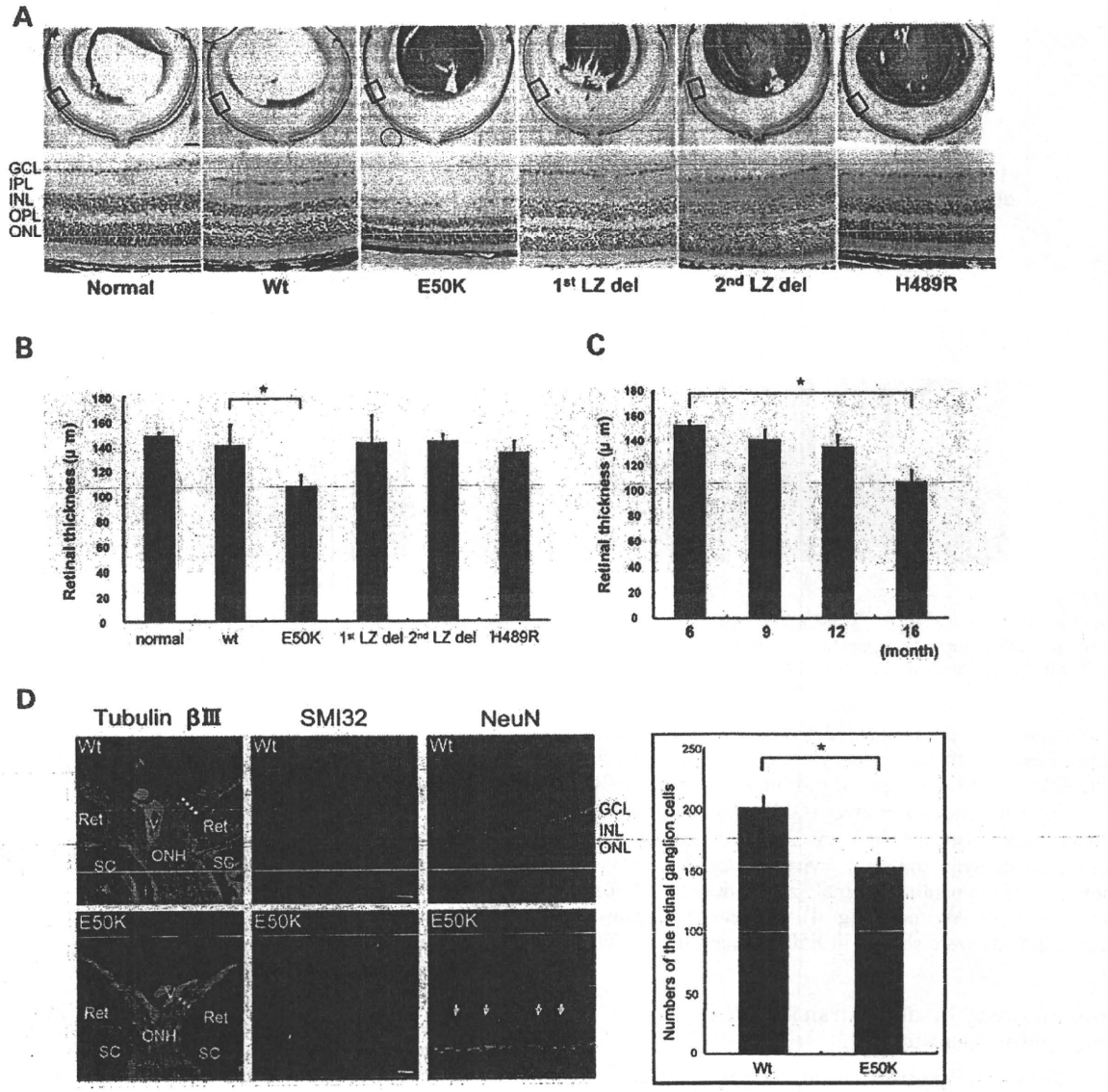

Figure 2. Comparison of retina morphology of normal, Wt and mutant transgenic mice. (**A**) HE staining of retina sections of 16-month-old normal and transgenic mice. Scale bar: 200 μm (upper panel), 50 μm (lower panel). (**B**) Quantification of the retina thickness measurements of different transgenic lines at 16 months of age. Six retina samples were measured in each group. Significant thinning of the retina was observed only for E50K mice ($^*P < 0.05$). (**C**) Quantification of the retina thickness measurements of E50K mice of different ages (6 to 16 months; $n = 6$ for each time point). E50K mice showed statistically significant retinal thinning at 16 months of age. (**D**) Tubulin β-III immunostaining of the Wt and E50K mice at the optic nerve head (scale bar: 50 μm). Reduction of the RGC number at the peripheral retina is shown by NeuN immunostaining of paraffin section and SMI32 immunostaining of flat mount retina for Wt and E50K mice (scale bar: 100 μm). RGCs were counted over entire paraffin sections for NeuN immunostaining. Right panel represents quantification of these results. Significant loss of the RGCs was observed in the E50K mice compared with Wt ($^*P < 0.05$).

(JOAG) (6,8–11,25–27). E50K, a substitution of glutamic acid by lysine at amino acid 50, is exclusively associated with the familial and sporadic forms of NTG (6,8,11), and that phenotype is, on an average, more severe compared with NTG without the E50K mutation (Supplementary Material) (6). A study by Hauser *et al.* (12) also reported a more severe glaucomatous phenotype in a patient with E50K mutation than that in the other NTG patient. The H486R mutation is reportedly associated with both NTG and JOAG (4,26). Histidine 486 is an evolutionarily conserved residue located at the C-terminus, where five other proteins, adenovirus E3-14.K, huntingtin, metabotrophic glutamate receptor 1-a, myosin VI, ring finger protein 11, can interact with Optn (Fig. 1A). On the other hand, we chose 1st and 2nd LZ del as the transgenic construct design. As shown in Figure 1A, both LZ regions are binding sites for various functional molecules—1st LZ: Rab8 and FOS; 2nd LZ: Huntingtin, E3-14.7K, Myosin6, mGluR1, RNF11. To elucidate the functional defect which may occur by deleting these regions, we generated 1st and 2nd LZ del transgenic mice.

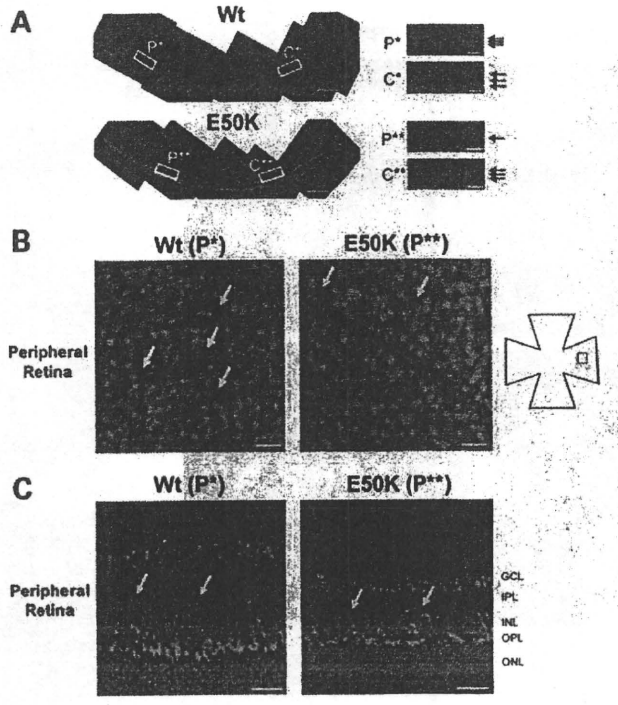

Figure 3. Changes in the retina of E50K mice. (**A**) Immunostaining of the retina sections with anti-calretinin antibody, a specific marker for RGCs and amacrine cells. Disruption of synapses between RGCs and amacrine cells was observed in the peripheral retina of E50K but not control mice (yellow box, P**). Scale bar: 20 μm. (**B**) Immunostaining of the flat mount retina with ChAT (red) and NeuN (green). A significant number of starburst amacrine cells were lost in the RGC layer in the peripheral retina of E50K mutant mice (P**) compared with Wt mice (P*). Scale bar: 50 μm. (**C**) Immunostaining of the retina sections with tyrosine hydroxylase (red) and PKC α (green), specific markers for dopaminergic amacrine cells and rod bipolar cells, respectively. Amacrine cell loss and size reduction of bipolar cells were observed. Scale bar: 20 μm.

Taken together, we hypothesized that each OPTN transgenic line would show distinct phenotype because of different locations of mutations, influencing different OPTN-interacting proteins. Surprisingly, only E50K mutant showed severe histopathological changes in mice. The E50K mice showed not only loss of RGCs, but also progressive retinal degeneration exclusively in the peripheral region (Figs. 2–4). Immunolabeling of ssDNA demonstrated that apoptotic changes occurred in all retinal cell layers. The number of cells in different retinal layers, including amacrine, bipolar and photoreceptor cells, and thickness of all retinal cell layers were reduced in the peripheral retina of E50K mice.

Herein, a question may rise from these findings in E50K mice: why is neuronal degeneration eminent at the peripheral retina, not at the central retina? Previous reports have indicated that mouse models of glaucoma follow similar natural courses of peripheral retinal degeneration. These include the well-known glaucoma mouse model, the DBA/2J mouse, and recently reported GLAST-deficient mouse, where all layers of the peripheral retina were shown to be affected, leading to a significant reduction of retinal thickness (24,28). The myocilin Tyr437His transgenic mouse, a POAG mouse model, also develops RGC loss at the peripheral retina and retinal degeneration (29,30). These three mouse models all share a pattern of peripheral degeneration with Optn E50K mice. In general, glaucoma most often affects peripheral visual field at early stages of the disease, whereas deterioration of the central retina can be seen only at later stages of the disease (31). We can speculate that the increased sensitivity of peripheral RGCs is associated with longer non-myelinated axons compared with the central RGCs, but this would not explain the degeneration of other neuronal cells. Further investigation is required to explain the difference of E50K susceptibility between mouse and human at the peripheral retina. The fact that E50K mice develop a phenotype of peripheral RGC degeneration which is similar to the previous glaucoma mouse models suggests that later stages of cellular and molecular mechanisms for neuronal degeneration are shared between NTG and POAG. Therefore, the use of E50K mice in exploring the mechanisms of NTG pathogenesis, as well as the development of new therapeutic interventions, holds great promise.

Rab8 belongs to a family of small GTP-binding proteins which act as regulators of multiple cellular processes. Rab GTPases regulate all stages of membrane trafficking, including vesicle transport, cargo sorting, transport, tethering and fusion (32). Rab8 has been shown to be involved in polarized membrane transport and regulation of vesicular transport from the trans-Golgi network (33). Recently, OPTN was demonstrated to protect survival of NIH3T3 cells under oxidative stress by relocating to the nucleus in an Rab8-dependent manner, whereas E50K lost the ability to translocate to the nucleus (34). These previous functional analyses of the protein–protein interaction reveal that OPTN–Rab8 complex is involved in multiple functions that are essential for retinal and optic nerve health. Thus, alterations of this complex by E50K mutation may influence the entire cellular function, leading to glaucomatous-like pathology.

Our study demonstrated for the first time a direct protein–protein interaction of OPTN and Rab8 at the Golgi-complex and spreading vesicles (Fig. 6C), which was completely abolished by E50K mutation. The downstream effect of this disruption can be predicted by two studies by Buss and colleagues and Canals and colleagues, who demonstrated the importance of OPTN–Rab8 complex with myosin VI or huntingtin for post-Golgi trafficking, respectively (18,35). Sahlendaer *et al.* (18) demonstrated that OPTN and active Rab8 interact with myosin VI and this is essential for the formation of Golgi ribbon and exocytosis. del Toro *et al.* (35) demonstrated that a mutation in huntingtin reduces interaction with OPTN–Rab8 complex, resulting in delocalization of the complex in Golgi and impairment of post-Golgi trafficking. In both studies, OPTN–Rab8 was considered essential component of post-Golgi trafficking system, whereas OPTN served as an effecter protein of Rab8 and a binding partner of the actin-based motor protein myosin VI. Disruption of this complex may result in a significant reduction of selected protein transport within the cell and to the cell surface for secretion. It would be interesting to investigate what type of cargo is affected by the E50K mutation and if cells be rescued by supplementing this cargo molecule. If these proteins can be

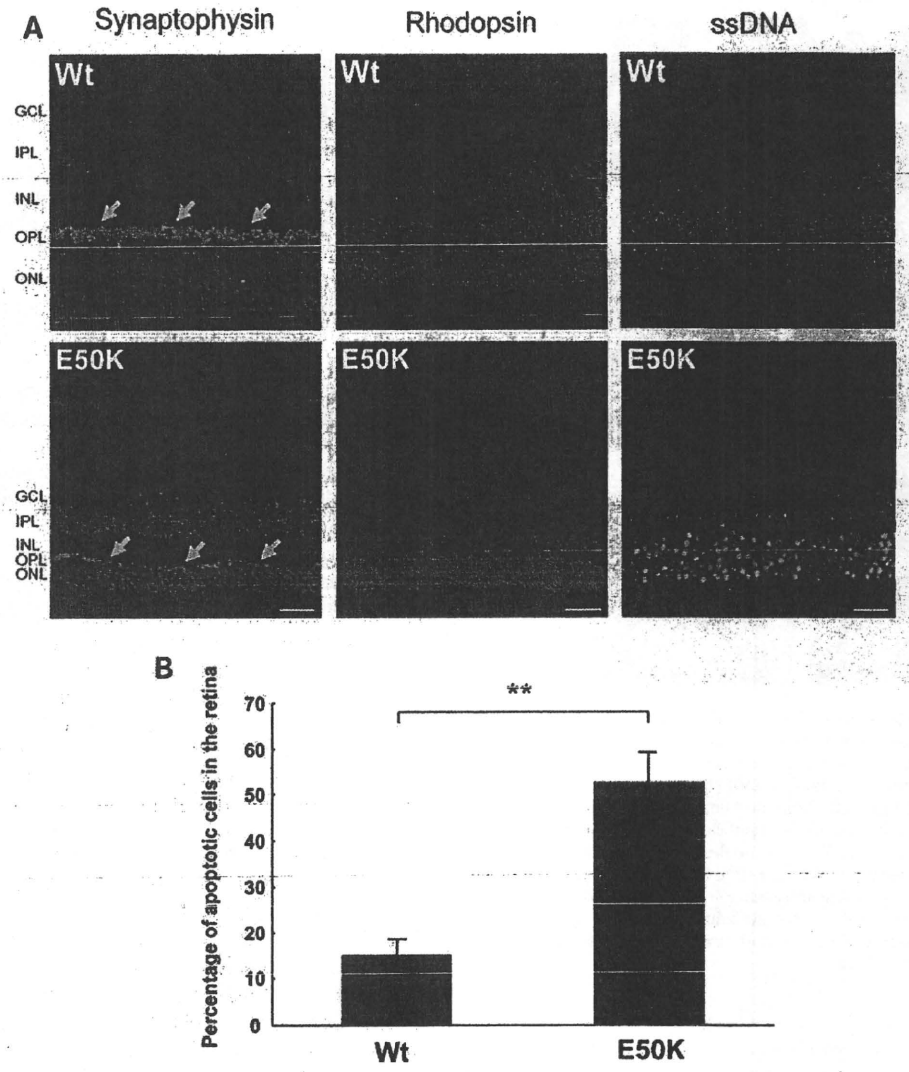

Figure 4. Degeneration of the OPL and ONL in the peripheral retina of E50K mice. (**A**) Immunostaining of the retina sections with synaptophysin, rhodopsin and ssDNA, specific markers for neuronal presynaptic vesicles, rod photoreceptors and apoptosis cells, respectively. Synapse disruption (arrow), rod photoreceptor cells degeneration and apoptosis cells were observed in the OPL and/or ONL in the peripheral retina of E50K mice. Scale bar: 20 μm. (**B**) Percentage of apoptotic cells in the ONL ($n = 6$, $^{**}P < 0.01$).

identified; it may serve as potential therapeutic approach to treat glaucoma patients with E50K mutation.

In the photoreceptor, Rab8 has a pivotal role of docking and fusion in rhodopsin trafficking (36) and cooperating with Bardet–Biedl syndrome proteins in ciliary membrane biogenesis (37,38). One possible explanation about the significant apoptotic changes in the ONL suggests that disruption of OPTN–Rab8 complex may affect the trafficking not only in the RGCs but also in the photoreceptors. Until now, there are no reports about the correlation between OPTN and Rab8 in the photoreceptors, or OPTN-mutated glaucoma and photoreceptor function. Considering trafficking malfunction via OPTN mutation as the etiology of glaucoma, E50K mice provides a good animal model to explore the pathogenesis of RGC and photoreceptor.

MATERIALS AND METHODS

Cloning of mouse Optn and site-directed mutagenesis

Total RNA was extracted from a fresh C57BL/6N mouse brain tissue using TRIzol (Invitrogen, Carlsbad, CA, USA) and reverse-transcribed into first-strand cDNA using oligo-dT adaptor primer and SuperScript First-Strand Synthesis System for RT–PCR (Invitrogen). OPTN cDNA was amplified by PCR using oligonucleotides 5′-cggaattccgatgtcccatcaacctctgag-3′ and 5′-cggaattccgtcaaatgatgcagtccatca-3′ as primers. The amplified DNA fragment was purified using a MinElute gel extraction kit (Qiagen, Hilden, Germany), ligated into pBluescript II (KS-) (Agilent Technologies, Santa Clara, CA, USA) and sequenced using the M13 primers and ABI PRISM 3130 (Applied Biosystems, Foster City, CA, USA). Site-directed

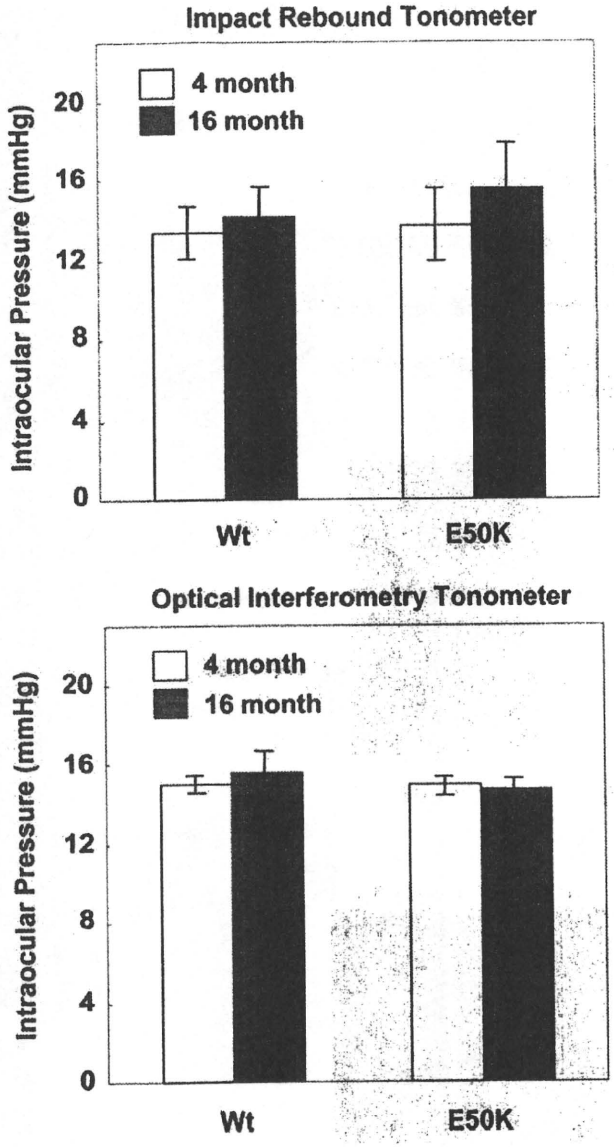

Figure 5. IOP measurement of Wt and E50K mice. IOP was measured using an impact-rebound tonometer and an optical interferometry tonometer between 9 AM and noon in 4-month and 16-month-old mice. Both methods gave similar results (IOP of 15 ± 1 mmHg) for Wt and transgenic mice at both ages examined ($n = 6$).

mutagenesis was carried out to produce cDNA corresponding to the deletion of the E50K mutation, the first leucine zipper (1st LZ del), deletion of the second leucine zipper (2nd LZ del) and the H489R mutation. The following primers were used: 5′-cagctcaaactcaactccgg-3′ and 5′-atgctccacttcctgctcca-3′ for 1st LZ del, 5′-aaatgaaggaactcctggttaagaaccaccagctgaaagaa-3′ and 5′-ttctttcagctggtggttcttaaccaggagttccttcattt-3′ for E50K, 5′-gagaccatggccgtcctc-3′ and 5′-caacatcttgtccaccttttctg-3′ for 2nd LZ del and 5′-gcagcaagagagaagattcgtgaagaaaaggagcagc-3′ and 5′-gctgctccttttcttcacgaatcttctctcttgctgc-3′ for H489R. Plasmids were digested with *Eco*RI, purified by agarose gel electrophoresis and recovered using the MinElute gel extraction kit according to the manufacturer's protocol. The cDNA inserts were ligated into *Eco*RI-digested pCMVHA vector (Takara Bio USA, Madison, WI, USA). HA-tagged Optns were amplified by PCR using oligonucleotides 5′-ccgctcgagcgccaccatgatg tacccatacgatgttcc-3′ and 5′-ccgctcgagcggtcaaatgatgcagtccatca-3′ as primers. HA-tag was inserted at the N-terminus of Optn constructs for the detection of proteins expressed by the transgene. The amplified DNA fragments were purified using a MinElute gel extraction kit (Qiagen), ligated into the expression vector and sequenced as described earlier.

Development of transgenic mice overexpressing mutant Optn

The expression vector pCAGGS containing chicken beta-actin promoter with CMV enhancer kindly provided by Dr Junichi Miyazaki of Osaka University was used for strong ubiquitous expression of the transgene in mice. cDNA inserts were released from the pCAGGS vector using *Sal*I and *Bam*HI. These restriction fragments were injected into pronuclear-stage BDF1/C57BL6N embryos, and transgenic mice were generated at PhoenixBio Co., Ltd (Tochigi, Japan). Offspring were screened for the transgene by isolating genomic DNA from tail biopsies followed by PCR. Primers used for PCR were 5′-ctctagagcctctgctaaccatgt-3′ and 5′-ccatggccataagagcg taa-3′. To determine copy number of transgenes, real-time PCR was performed using TaqMan MGB probe (Applied Biosystems), according to manufacturer's standard protocols. Primers and probe for the mouse beta-actin were 5′-AGGC CAACCGTGAAAAGATG-3′ (forward), 5′-TGAGAAGCTG GCCAAAGAGAA-3′ (reverse) and 5′-CCCAGGTCAGTAT CC-3′ (probe); for the CAG promoter were 5′-CCGCAGCC ATTGCCTTT-3′ (forward), 5′-TTCGGCTCCGCACAGATT-3′ (reverse) and 5′-CGCAGGGACTTCC-3′ (probe). To determine the absolute amount of the copy number of beta-actin, PCR products of mouse beta-actin amplified from genomic DNA were cloned into the pCAGGS vector. The copy number of beta-actin gene in mouse genome was measured with real-time PCR analyses, the purified plasmid DNAs were used as standards. To determine the transgene copy number, multiplex quantitative PCR was performed for both CAG promoter as a target and beta-actin gene as a reference. All experiments with mice were performed in accordance with the Association for Research in Vision and Ophthalmology Statement for the Use of Animals in Vision Research.

Histology and immunohistochemistry

Mice were sacrificed with Nembutal (150 mg/kg) i.p., and the eyes were removed quickly. For histology, mouse eyes were dissected and immersed in Davidson's solution fixative overnight at 4°C. The eyes were embedded in paraffin and sectioned at 5 μm thickness along the vertical meridian through the optic nerve head. After deparaffinization and rehydration, sections were stained with hematoxylin and eosin (HE) staining. Images of HE staining were collected with Nikon Eclipse light microscope (Nikon, Tokyo, Japan).

For immunohistochemistry, after deparaffinization and rehydration, eye sections were treated with Target Retrieval Solution (DakoCytomation, Denmark). These sections were incubated

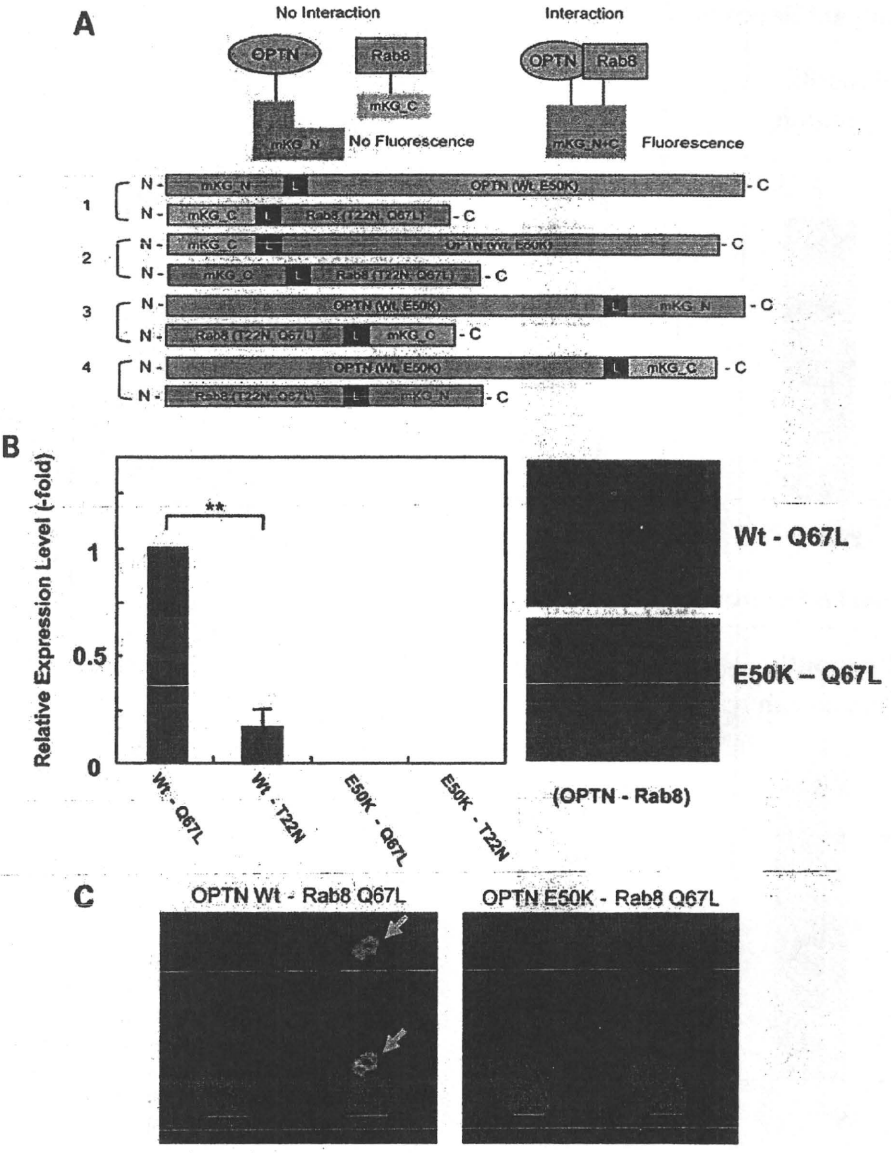

Figure 6. Disruption of OPTN–Rab8 interaction by the E50K mutation. (**A**) A diagram of cDNA constructs used in experiments to study protein–protein interaction. (**B**) The protein–protein interaction of OPTN Wt and E50K with Rab8 T22N (GDP inactive form), and Q67L (GTP active form) was measured in RGC-5 cells as described in Materials and Methods. Interaction of OPTN Wt and Q67L-active form of Rab8 was increased five times over Rab8 T22N-inactive form of Rab8 protein (**$P < 0.01$). E50K did not show any interaction with any construct including the active form of Rab8 ($n = 6$). (**C**) Co-localization of the OPTN–Rab8 complex (green) and Golgi marker GM130 (red). COS1 cells were transfected with constructs encoding indicated constructs and stained with antibodies against GM130 48 h after transfection as described in Materials and Methods. Nuclei (blue) were stained with DAPI.

with blocking solution for 1 h followed by overnight incubation with primary antibody against HA tag (1:500 dilution; Sigma-Aldrich, St Louis, MO, USA), OPTN (1:500 dilution; kind gift from Dr Mansoor Sarfarazi, University of Connecticut), tubulin β-III isoform (1:100 dilution; Millipore, Billerica, MA, USA), NeuN (1:100 dilution; Millipore), calretinin (1:500 dilution; Sigma), tyrosine hydroxylase (1:100 dilution; Millipore), PKC α (1:500 dilution; Millipore), rhodopsin (1:200 dilution; Santa Cruz, CA, USA), synaptophysin (1:500 dilution; Abcam, Cambridge, MA, USA) or ssDNA (1:500 dilution; Immuno-Biological Laboratories, Gunma, Japan) in phosphate-buffered saline (PBS) containing 1% BSA at 4°C. Slides were washed in PBS and then incubated with Alexa 488 or Alexa 568 (1:500 dilution; Invitrogen)-conjugated anti-mouse or rabbit IgG and 4′,6′-diamidino-2-phenylindole (DAPI) for nuclear staining for 1 h at room temperature. The stained tissues were examined using confocal fluorescence laser microscope (Radiance 2000, Bio-Rad Laboratories, Hercules, CA, USA). Control slides were processed similarly, except for the omission of primary antibodies (data not shown).

Whole-mount immunostaining

The whole-mount immunostaining was performed essentially as described (39,40). Briefly, neural retinas were separated from the posterior eyes, fixed in 4% PFA/PBS for 2 h on ice and incubated with the anti-SMI32 (1:200 dilution; Sternberger Monoclonals, Baltimore, MD, USA), anti-ChAT (1:100 dilution; Millipore) or anti-active NeuN (1:250 dilution; Millipore) antibody for 7 days at 4°C. Slides were washed in PBS containing 0.1% Triton X-100 and then incubated with Alexa 488 or Alexa 568 (1:500 dilution; Invitrogen)-conjugated anti-mouse or rabbit IgG/DAPI for 2 days at 4°C. Whole-mounted retinal samples were placed on slides, with the vitreous facing up. Radial cuts were made in the peripheral retina, and the retinal tissue was flattened with a fine brush. The retinas were then mounted with Vectashield (Vector Laboratories, Burlingame, CA, USA) and evaluated with a confocal microscope.

Measurement of IOP

The average IOP for each genotype was recorded. IOP was measured using an impact-rebound tonometer (Colonal Medical Supply, Franconia, NH, USA) and optical interferometry tonometer (FISO Technologies, Quebec, Canada) for mice of each genotype as described (29). Using the rebound tonometer, we were able to measure IOP in awake and non-sedated mice of various ages, whereas optical interferometry tonometry was performed on anesthetized animals. Measurement of IOP was always performed in the morning between 10 and 12 AM. The mice successfully assessed for each genotype and age were 18 weeks and 16 months.

Measurement of OPTN–Rab8 interaction

OPTN–Rab8 interaction analysis was performed using Coral-Hue® Fluo-chase Kit (MBL, Tokyo, Japan). Based on the instruction manual, we constructed OPTN Wt, E50K, Rab8 Q67L (GTP-bound active form), Rab8 T22N (GDP-bound inactive form), with fluorescence tag protein (mKG_N or mKG_C) on either N-terminal or C-terminal (Fig. 6A). RGC-5 and COS1 cells were transfected by each pair of the plasmid mixtures using Fugene HD (Roche Diagnostics, Mannheim, Germany). Forty-eight hours after transfection, the medium was replaced to PBS and the cells were observed with inverted microscope (Eclipse TE300, Nikon). To observe localization of OPTN–Rab8 complex, cells were fixed 48 h after transfection with 4% paraformaldehyde in PBS on ice for 20 min. Cells were incubated in blocking buffer (3% bovine serum albumin, 0.1% Triton X-100 in PBS) and then with anti-GM130 antibody (BD Bioscience, San Jose, CA, USA) at room temperature for 1 h each. Cells were washed three times with PBS-T (0.1% Triton X-100 in PBS) and incubated with Alexa-568-conjugated secondary antibody for 1 h at room temperature. Slides were washed, mounted and analyzed by confocal microscopy.

Statistical analysis

All data were expressed as the mean ± standard deviation. Statistical differences were analyzed by the ANOVA or Student's *t*-test. $^*P < 0.05$ was considered statistically significant.

SUPPLEMENTARY MATERIAL

Supplementary Material is available at *HMG* online.

ACKNOWLEDGEMENTS

The authors thank T.V. Johnson, S. Zigler, Jr, for critical reading of the manuscript and K. Fujinami for helpful comments.

Conflict of Interest statement. None declared.

FUNDING

This research was supported in part by the grants to T.I. by the Japan Ministry of Health, Labor, and Welfare, to T.I. and M.A. by the Japan Ministry of Education, Culture, Sports, Science and Technology and to T.I. for Japan Society for the Promotion Science Fellowship for Z.C. Funding to pay the Open Access publication charges for this article was provided by the Japan Ministry of Health, Labor, and Welfare.

REFERENCES

1. Quigley, H.A. (1996) Number of people with glaucoma worldwide. *Br. J. Ophthalmol.*, **80**, 389–393.
2. Quigley, H.A. and Broman, A.T. (2006) The number of people with glaucoma world wide in 2010 and 2020. *Br. J. Ophthalmol.*, **90**, 262–267.
3. Iwase, A., Suzuki, Y., Araie, M., Yamamoto, T., Abe, H., Shirato, S., Kuwayama, Y., Mishima, H.K., Shimizu, H., Tomita, G. *et al.* (2004) The prevalence of primary open-angle glaucoma in Japanese: the Tajimi Study. *Ophthalmology*, **111**, 1641–1648.
4. Stone, E.M., Fingert, J.H., Alward, W.L., Nguyen, T.D., Polansky, J.R., Sunden, S.L., Nishimura, D., Clark, A.F., Nystuen, A., Nichols, B.E. *et al.* (1997) Identification of a gene that causes primary open angle glaucoma. *Science*, **275**, 668–670.
5. Stoilov, I., Akarsu, A.N. and Sarfarazi, M. (1997) Identification of three different truncating mutations in cytochrome P4501B1 (CYP1B1) as the principal cause of primary congenital glaucoma (buphthalmos) in families linked to the GLC3A locus on chromosome 2p21. *Hum. Mol. Genet.*, **6**, 641–647.
6. Rezaie, T., Child, A., Hitchings, R., Brice, G., Miller, L., Coca-Prados, M., Heon, E., Krupin, T., Ritch, R., Kreutzer, D. *et al.* (2002) Adult-onset primary open-angle glaucoma caused by mutations in optineurin. *Science*, **295**, 1077–1079.
7. Monemi, S., Spaeth, G., DaSilva, A., Popinchalk, S., Ilitchev, E., Liebmann, J., Ritch, R., Heon, E., Crick, R.P., Child, A. *et al.* (2005) Identification of a novel adult-onset primary open-angle glaucoma (POAG) gene on 5q22.1. *Hum. Mol. Genet.*, **14**, 725–733.
8. Aung, T., Rezaie, T., Okada, K., Viswanathan, A.C., Child, A.H., Brice, G., Bhattacharya, S.S., Lehmann, O.J., Sarfarazi, M. and Hitchings, R.A. (2005) Clinical features and course of patients with glaucoma with the E50K mutation in the optineurin gene. *Invest. Ophthalmol. Vis. Sci.*, **46**, 2816–2822.
9. Leung, Y.F., Fan, B.J., Lam, D.S., Lee, W.S., Tam, P.O., Chua, J.K., Tham, C.C., Lai, J.S., Fan, D.S. and Pang, C.P. (2003) Different optineurin mutation pattern in primary open-angle glaucoma. *Invest. Ophthalmol. Vis. Sci.*, **44**, 3880–3884.
10. Fuse, N., Takahashi, K., Akiyama, H., Nakazawa, T., Seimiya, M., Kuwahara, S. and Tamai, M. (2004) Molecular genetic analysis of optineurin gene for primary open-angle and normal tension glaucoma in the Japanese population. *J. Glaucoma*, **13**, 299–303.
11. Alward, W.L., Kwon, Y.H., Kawase, K., Craig, J.E., Hayreh, S.S., Johnson, A.T., Khanna, C.L., Yamamoto, T., Mackey, D.A., Roos, B.R. *et al.* (2003) Evaluation of optineurin sequence variations in 1,048 patients with open-angle glaucoma. *Am. J. Ophthalmol.*, **136**, 904–910.

12. Hauser, M.A., Sena, D.F., Flor, J., Walter, J., Auguste, J., Larocque-Abramson, K., Graham, F., Delbono, E., Haines, J.L., Pericak-Vance, M.A. *et al.* (2006) Distribution of optineurin sequence variations in an ethnically diverse population of low-tension glaucoma patients from the United States. *J. Glaucoma*, **15**, 358–363.
13. Chalasani, M.L., Radha, V., Gupta, V., Agarwal, N., Balasubramanian, D. and Swarup, G. (2007) A glaucoma-associated mutant of optineurin selectively induces death of retinal ganglion cells which is inhibited by antioxidants. *Invest. Ophthal. Vis. Sci.*, **48**, 1607–1614.
14. Faber, P.W., Barnes, G.T., Srinidhi, J., Chen, J., Gusella, J.F. and MacDonald, M.E. (1998) Huntingtin interacts with a family of WW domain proteins. *Hum. Mol. Genet.*, **7**, 1463–1474.
15. Moreland, R.J., Dresser, M.E., Rodgers, J.S., Roe, B.A., Conaway, J.W., Conaway, R.C. and Hanas, J.S. (2000) Identification of a transcription factor IIIA-interacting protein. *Nucleic Acids Res.*, **28**, 1986–1993.
16. Hattula, K. and Peranen, J. (2000) FIP-2, a coiled-coil protein, links Huntingtin to Rab8 and modulates cellular morphogenesis. *Curr. Biol.*, **10**, 1603–1606.
17. Park, B.C., Shen, X., Samaraweera, M. and Yue, B.Y. (2006) Studies of optineurin, a glaucoma gene: Golgi fragmentation and cell death from overexpression of wild-type and mutant optineurin in two ocular cell types. *Am. J. Pathol.*, **169**, 1976–1989.
18. Sahlender, D.A., Roberts, R.C., Arden, S.D., Spudich, G., Taylor, M.J., Luzio, J.P., Kendrick-Jones, J. and Buss, F. (2005) Optineurin links myosin VI to the Golgi complex and is involved in Golgi organization and exocytosis. *J. Cell. Biol.*, **169**, 285–295.
19. Miyamoto-Sato, E., Ishizaka, M., Horisawa, K., Tateyama, S., Takashima, H., Fuse, S., Sue, K., Hirai, N., Masuoka, K. and Yanagawa, H. (2005) Cell-free cotranslation and selection using *in vitro* virus for high-throughput analysis of protein–protein interactions and complexes. *Genome Res.*, **15**, 710–717.
20. Colland, F., Jacq, X., Trouplin, V., Mousin, C., Groizeleau, C., Hamburger, A., Meil, A., Wojcik, J., Legrain, P. and Gauthier, J.M. (2004) Functional proteomics mapping of a human signaling pathway. *Genome Res.*, **14**, 1324–1332.
21. Anborgh, P.H., Godin, C., Pampillo, M., Dhami, G.K., Dale, L.B., Cregan, S.P., Truant, R. and Ferguson, S.S. (2005) Inhibition of metabotropic glutamate receptor signalling by the huntingtin binding protein optineurin. *J. Biol. Chem.*, **280**, 34840–34848.
22. Sudhakar, C., Nagabhushana, A., Jain, N. and Swarup, G. (2009) NF-kappaB mediates tumor necrosis factor alpha-induced expression of optineurin, a negative regulator of NF-kappaB. *PLoS One*, **4**, e5114.
23. Journo, C., Filipe, J., About, F., Chevalier, S.A., Afonso, P.V., Brady, J.N., Flynn, D., Tangy, F., Israël, A. and Vidalain, P.O. (2009) NRP/optineurin cooperates with TAX1BP1 to potentiate the activation of NF-kappaB by human T-lymphotropic virus type 1 tax protein. *PLoS Pathog.*, **5**, e1000521.
24. Harada, T., Harada, C., Nakamura, K., Quah, H.M., Okumura, A., Namekata, K., Saeki, T., Aihara, M., Yoshida, H., Mitani, A. *et al.* (2007) The potential role of glutamate transporters in the pathogenesis of normal tension glaucoma. *J. Clin. Invest.*, **117**, 1763–1770.
25. Funayama, T., Ishikawa, K., Ohtake, Y., Tanito, T., Kurosaka, D., Kimura, I., Suzuki, K., Ideta, H., Nakamoto, K., Yasuda, N. *et al.* (2004) Variants in optineurin gene and their association with tumor necrosis factor-alpha polymorphisms in Japanese patients with glaucoma. *Invest. Ophthalmol. Vis. Sci.*, **45**, 4359–4367.
26. Weisschuh, N., Neumann, D., Wolf, C., Wissinger, B. and Gramer, E. (2005) Prevalence of myocilin and optineurin sequence variants in German normal tension glaucoma patients. *Mol. Vis.*, **11**, 284–287.
27. Yao, H.Y., Cheng, C.Y., Fan, B.J., Tam, O.S., Tham, C.Y., Wang, D.Y., Lam, S.C. and Pang, C.P. (2006) Polymorphisms of myocilin and optineurin 1 primary open-angle glaucoma patients. *Zhonghua Yi Xue Za Zhi.*, **86**, 554–559.
28. John, S.W., Smith, R.S., Savinova, O.V., Hawes, N.L., Chang, B., Turnbull, D., Davisson, M., Roderick, T.H. and Heckenlively, J.R. (1998) Essential iris atrophy, pigment dispersion, and glaucoma in DBA/2J mice. *Invest. Ophthalmol. Vis. Sci.*, **39**, 951–962.
29. Senatorov, V., Malyukova, I., Fariss, R., Wawrousek, E.F., Swaminathan, S., Sharan, S.K. and Tomarev, S. (2006) Expression of mutated mouse myocilin induces open-angle glaucoma in transgenic mice. *J. Neurosci.*, **26**, 11903–11914.
30. Zhou, Y., Grinchuk, O. and Tomarev, S.I. (2008) Transgenic mice expressing the Tyr437His mutant of human myocilin protein develop glaucoma. *Invest. Ophthalmol. Vis. Sci.*, **49**, 1932–1939.
31. Foster, P.J., Buhrmann, R., Quigley, H.A. and Johnson, G.J. (2002) The definition and classification of glaucoma in prevalence surveys. *Br. J. Ophthalmol.*, **86**, 238–242.
32. Zerial, M. and McBride, H. (2001) Rab proteins as membrane organizers. *Nat. Rev. Mol. Cell. Biol.*, **2**, 107–117.
33. Huber, L.A., Pimplikar, S., Parton, R.G., Virta, H., Zerial, M. and Simons, K. (1993) Rab8, a small GTPase involved in vesicular traffic between the TGN and the basolateral plasma membrane. *J. Cell. Biol.*, **123**, 35–45.
34. De Marco, N., Buono, M., Troise, F. and Diez-Roux, G. (2006) Optineurin increases cell survival and translocates to the nucleus in a Rab8-dependent manner upon an apoptotic stimulus. *J. Biol. Chem.*, **281**, 16147–16156.
35. del Toro, D., Alberch, J., Lázaro-Diéguez, F., Martín-Ibáñez, R., Xifró, X., Egea, G. and Canals, J.M. (2009) Mutant huntingtin impairs post-Golgi trafficking to lysosomes by delocalizing optineurin/Rab8 complex from the Golgi apparatus. *Mol. Biol. Cell.*, **20**, 1478–1492.
36. Moritz, O.L., Tam, B.M., Hurd, L.L., Peranen, J., Deretic, D. and Papermaster, D.S. (2001) Mutant rab8 impairs docking and fusion of rhodopsin-bearing post-Golgi membranes and causes cell death of transgenic *Xenopus* rods. *Mol. Biol. Cell.*, **12**, 2341–2351.
37. Sato, T., Mushiake, S., Kato, Y., Sato, K., Sato, M., Takeda, N., Ozono, K., Miki, K., Kubo, Y., Tsuji, A. *et al.* (2007) The Rab8 GTPase regulates apical protein localization in intestinal cells. *Nature*, **448**, 366–369.
38. Nachury, M.V., Loktev, A.V., Zhang, Q., Westlake, C.J., Peränen, J., Merdes, A., Slusarski, D.C., Scheller, R.H., Bazan, J.F., Sheffield, V.C. *et al.* (2007) A core complex of BBS proteins cooperates with the GTPase Rab8 to promote ciliary membrane biogenesis. *Cell*, **129**, 1201–1213.
39. Jakobs, T.C., Libby, R.T., Ben, Y., John, S.W. and Masland, R.H. (2005) Retinal ganglion cell degeneration is topological but not cell type specific in DBA/2J mice. *J. Cell Biol.*, **171**, 313–325.
40. Howell, G.R., Libby, R.T., Jakobs, T.C., Smith, R.S., Phalan, F.C., Barter, J.W., Barbay, J.M., Marchant, J.K., Mahesh, N., Porciatti, V. *et al.* (2007) Axons of retinal ganglion cells are insulted in the optic nerve early in DBA/2J glaucoma. *J. Cell Biol.*, **179**, 1523–1537.

HMG Advance Access published August 6, 2010

Human Molecular Genetics, 2010 *1–10*
doi:10.1093/hmg/ddq299

Mutant WDR36 directly affects axon growth of retinal ganglion cells leading to progressive retinal degeneration in mice

Zai-Long Chi[1], Fumie Yasumoto[1], Yuri Sergeev[2], Masayoshi Minami[1], Minoru Obazawa[1], Itaru Kimura[1], Yuichiro Takada[1] and Takeshi Iwata[1,*]

[1]Division of Molecular and Cellular Biology, National Institute of Sensory Organs, National Hospital Organization Tokyo Medical Center, 2-5-1 Higashigaoka, Meguro-ku, Tokyo 152-8902, Japan and [2]Ophthalmic Genetics and Visual Function Branch, National Eye Institute, National Institutes of Health, Building 10, Room 10N226, 10 Center Drive, MSC 1860, Bethesda, MD 20892-1860, USA

Received May 10, 2010; Revised June 14, 2010; Accepted July 12, 2010

Primary open-angle glaucoma (POAG) is one of the three principal subtypes of glaucoma and among the leading cause of blindness worldwide. POAG is defined by cell death of the retinal ganglion cells (RGCs) and surrounding neuronal cells at higher or normal intraocular pressure (IOP). Coded by one of the three genes responsible for POAG, WD repeat-containing protein 36 (WDR36) has two domains with a similar folding. To address whether WDR36 is functionally important in the retina, we developed four transgenic mice strains overexpressing a wild-type (Wt) and three mutant variants of D606G, deletion of amino acids at positions 605–607 (Del605–607) and at 601–640 (Del601–640) equivalent to the location of the D658G mutation observed in POAG patients. A triple amino acid deletion of mouse Wdr36 at positions 605–607 corresponding to the deletion at positions 657–659 in humans developed progressive retinal degeneration at the peripheral retina with normal IOP. RGCs and connecting amacrine cell synapses were affected at the peripheral retina. Axon outgrowth rate of cultured RGC directly isolated from transgenic animal was significantly reduced by the Wdr36 mutation compared with Wt. Molecular modeling of wild and mutant mouse Wdr36 revealed that deletion at positions 605–607 removed three residues and a hydrogen bond, required to stabilize anti-parallel β-sheet of the 6th β-propeller in the second domain. We concluded that WDR36 plays an important functional role in the retina homeostasis and mutation to this gene can cause devastating retinal damage. These data will improve understanding of the functional property of WDR36 in the retina and provide a new animal model for glaucoma therapeutics.

INTRODUCTION

Glaucoma is characterized by progressive loss of retinal ganglion cells (RGCs), degeneration of axons in the optic nerve leading to visual field defects. Primary open-angle glaucoma (POAG) is one of the major causes of irreversible blindness leading to 12% of all global blindness and by the year 2020 over 11 million people are predicted to be affected (1,2). POAG is often associated with elevated intraocular pressure (IOP) >21 mmHg, which becomes a major contributory factor for typical glaucomatous changes, including optic nerve head cupping and visual field loss. At present, at least 24 different loci have been linked to various forms of glaucoma and over a decade, three genes, myocilin (*MYOC*), optineurin (*OPTN*) and WD repeat-containing protein 36 (*WDR36*), have been identified as monogenic genes associated with POAG (3–5). *WDR36* was identified in the POAG loci GLC1G at 5q22.1 with segregation to POAG in the original paper (5). Hauser *et al.* (6) reported correlations of *WDR36* variants and POAG severity, while others described disease-causing variants at equal frequency as the

*To whom correspondence should be addressed. Tel/Fax: +81 334111026; Email: iwatatakeshi@kankakuki.go.jp

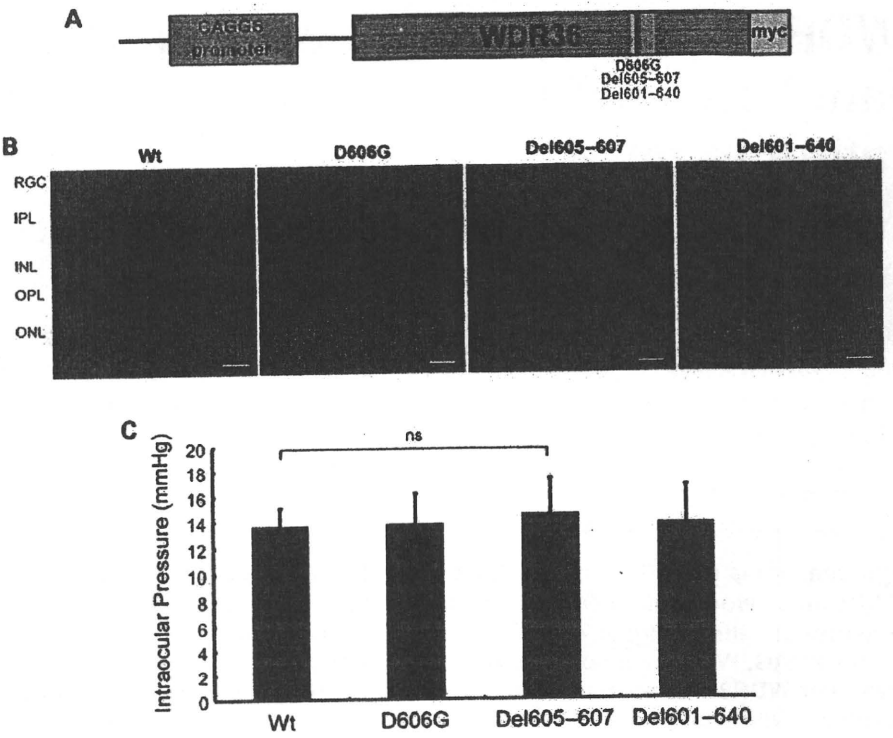

Figure 1. Development of *Wdr36* transgenic mouse. (A) Schematic diagram of the mouse *Wdr36* construct used in this study. Positions of mutations and deletions are shown. **(B)** Expression of each mutant Wdr36 was immunostained with anti-myc (red) and anti-Wdr36 (green) antibody. Image shown are co-localized. Scale bar, 20 μm. (C) IOP was measured at 16 months during 10 am to noon using impact-rebound tonometer. This method gave normal range for all transgenic mice ($n = 6$).

control (7–9). These mixed results suggest that *WDR36* may act as a modifier gene for POAG or only be responsible for selective familial POAG as in *MYOC* and *OPTN* variants (6,8).

WDR36 is a 100 kDa protein, containing multiple guanine nucleotide-binding WD40 repeats (WDR), an AMP-dependent synthetase and ligase, and a cytochrome cd1-nitrite reductase-like WD40-associated domain (5). Previous studies have shown that the loss of WDR36 activated the p53 stress–response pathway that disrupts nucleolar morphology and rRNA processing, resulting in a decrease of the 18S rRNA mature form (10). *Wdr36* knockout in zebrafish developed abnormal gut and smaller eye with progressive degeneration of the lens development. Homology modeling by Footz *et al.* (11) showed WDR36 containing 14 WDR, likely to fold in two connected seven-bladed β-propeller domains. WDR36 is ubiquitously expressed in all tissues and shares sequence homology with yeast Utp21. It is localized to the nucleoli and cytoplasm (10). Footz *et al.* further described that POAG-causing variants in WDR36 did not produce any significant defects in yeast viability or tRNA processing, but when combined with disruption of STI1, which synthetically interacts with UTP21, 5 of the 11 variants had increased or decreased cell viability due to reduced or elevated levels of pre-rRNA (11). These WDR36 variants included ones found in control populations, suggesting WDR36 as a modifier gene that requires another gene defect or unknown risk factor for the onset of POAG.

In this paper, we focused at the functionally sensitive site in the two 7-bladed β-propeller structure studied previously in humans and yeast. Overexpression of mutant Wdr36 produce significant and specific retinal damage in mice. Molecular modeling of wild-type (Wt) and mutant Wdr36 mice revealed explanation for the phenotypic results obtained in this study.

RESULTS

Construction of Wt and mutant Wdr36 transgenic mice

Four independent transgenic mice lines overexpressing Wt, D606G, deletion of amino acid 605–607 (Del605–607) located in seventh β-propeller in the second domain, and at positions 601–640 (Del601–640), a deletion of the entire seventh β-propeller of same domain, were developed independently in B7D2F1 (DBA/2J+C57BL/6J) mouse strain (Fig. 1A). The copy number of each mutant cDNA construct per mouse was approximately two to four, determined by TaqMan real-time polymerase chain reaction (PCR) assay (data not shown). The D606G is equivalent to the D658G mutation preferentially found in patients with POAG (5). Ubiquitous expression and distribution of Wt and mutant Wdr36 protein was visualized by immunostaining of myc-tag peptides fused to each *Wdr36* construct (Fig. 1B).

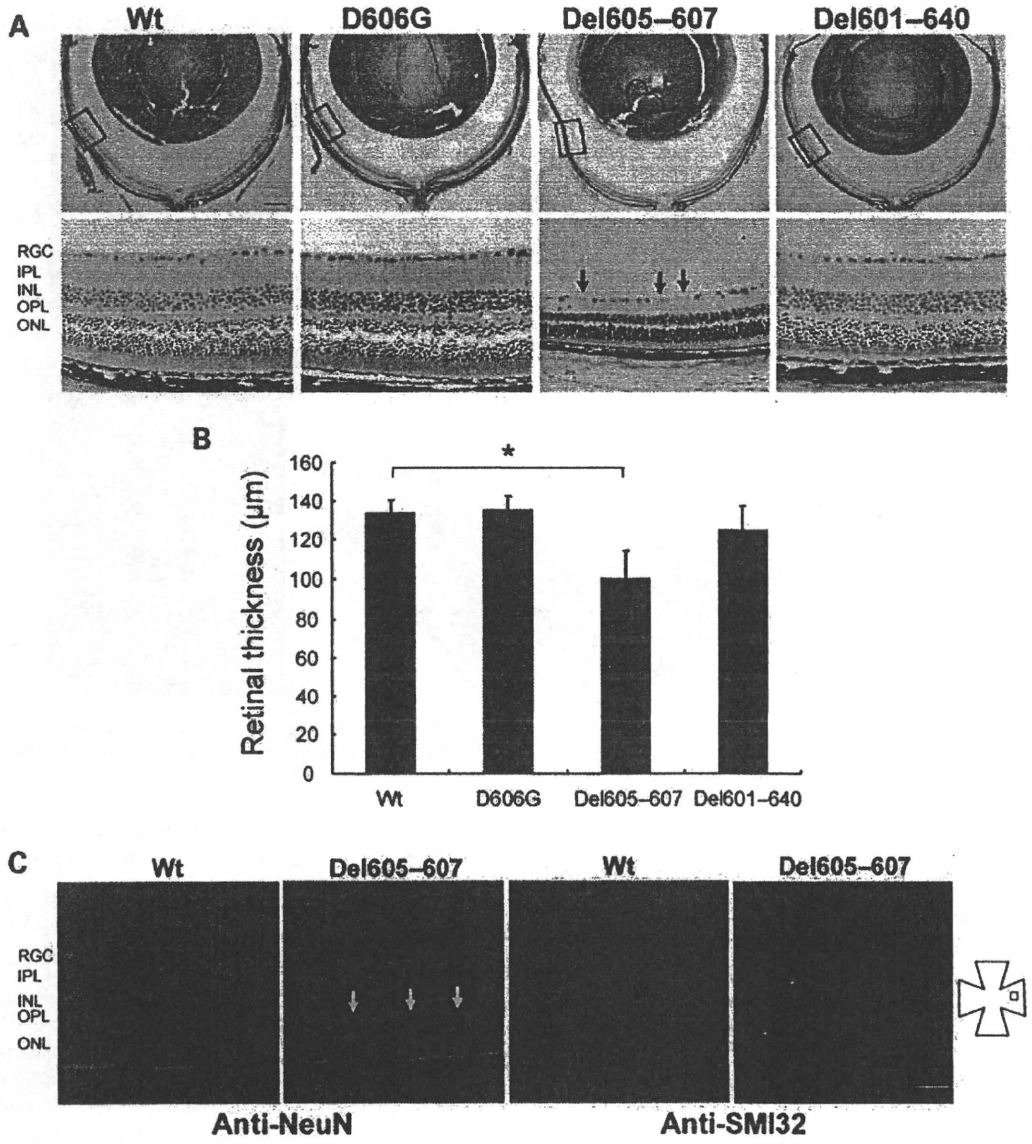

Figure 2. Comparison of retina morphology of Wt and mutant transgenic mice at the peripheral retina. (**A**) Hematoxylin–eosin staining of retina section is shown for 16-month-old transgenic mice. Scale bar, 200 μm (upper panel), 20 μm (lower panel). (**B**) Quantification of the retina thickness and RGC numbers of 16-month-old transgenic mice ($n = 6$). Significant thinning of the retina and loss of the RGCs (arrow) was specifically observed for Del605–607 mice ($^*P < 0.05$). RGC numbers was counted in the NeuN-immunostained paraffin section. (**C**) Reduction of RGC number at the peripheral retina (asterisks) is shown by NeuN immunostaining (green, scale bar 50 μm) of paraffin section and SMI32 immunostaining (red, scale bar 100 μm) of flat mount retina for Wt and Del605–607 mice.

IOP measurement for Wt and mutant mice

Elevated IOP is one of the major risk factors for glaucoma. We measured IOP in Wt and transgenic mice using noninvasive impact-rebound tonometer as described previously (12). The average IOP for Wt, D606G and Del601–640 was similar and in the normal range of approximately 13 mmHg at all examined ages (Fig. 1C). The Del605–607 mice gave a slight increase of IOP but statistically non-significant compared with other strains.

Histological comparison of Wt and mutant Wdr36 transgenic mice eye

Hematoxylin–eosin (H&E) staining of the entire eye section showed no obvious abnormality for mice over expressing Wt, D606G and Del601–640. However, significant change was observed for Del605–607 mice exclusively in the peripheral retina at 16 months of age (Fig. 2A). Approximately 25% reduction in the peripheral retina thickness was observed for Del605–607 mice compared with the Wt mice ($^*P < 0.05$;

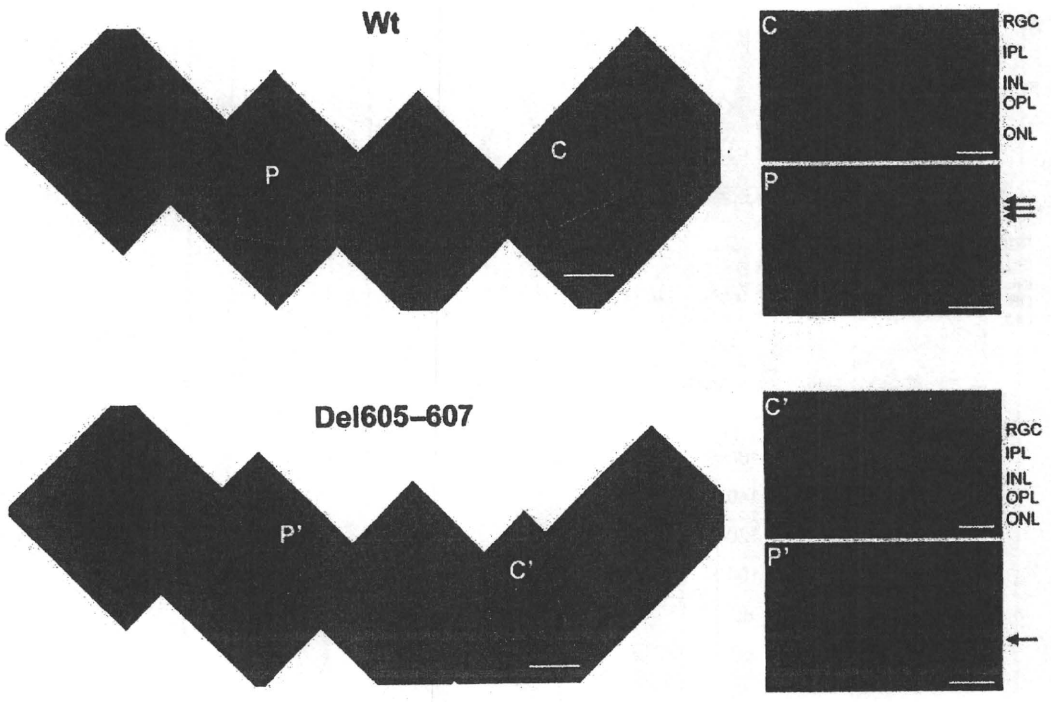

Figure 3. Disruption of synapses between RGC and amacrine cells in Del605–607 mice. Immunostaining of the retina sections with anti-calretinin antibody, a specific marker for RGCs and amacrine cells. Disruption of synapses between RGC and amacrine cells was specifically observed in peripheral (P) retina for Del605–607 mouse (P′) but not in the central (C) retina. Scale bar, 20 μm.

Fig. 2B). To maintain statistical quality, the measurements of retinal thickness were collected at the peripheral retina ~1.0–1.2 mm from the optic nerve head. Within the same peripheral region, RGC loss was observed by immunostaining with anti-NeuN, a neuron-specific marker, and counted through the entire retina sections (Fig. 2C). RGC loss at the peripheral retina was placed horizontally and visualized by anti-SMI32 immunostaining of the whole-mount retina in Del605–607 mice in comparison with Wt mice (Fig. 2C). Cornea, lens and the anterior segment of Del605–607 mice eye were histologically normal even after 16 months.

Histopathological evaluation of the retinal layers in Wdr36 Del605–607 mice

To determine which retinal cell components are vulnerable to the Del605–607 deletion, we performed immunohistochemical analysis using retinal cell-specific markers. In the inner plexiform layer (IPL), synapses of RGC and amacrine cells were visualized by calretinin immunostaining of retina sections of Wt and Del605–607 mice at 16 months (Fig. 3). A significant degeneration was observed in the peripheral retina in Del605–607 mice (Fig. 3, Panel P′) in contrast to the central retina of Wt and Del605–607 mice (Fig. 3, Panel C′). Loss of another type of amacrine cells and rod bipolar cells in the peripheral retina between the Del605–607 and Wt was detected by staining with antibodies against tyrosine hydroxylase (red, dopaminergic amacrine cell) and PKC α (green, rod bipolar cell) (Fig. 4A). Loss and/or abnormality of amacrine cells and bipolar cells was also observed in the Del605–607 mice. Expression of synaptophysin, a synaptic vesicle marker, was reduced in the outer plexiform layer (OPL) in Del605–607 mice compare with Wt mice (Fig. 4A).

Apoptosis assay by single-stranded DNA immunohistochemistry

Apoptotic cell death of RGC is one of the hallmarks of glaucoma pathogenesis. To visualize the apoptotic event in Wt and Del605–607 mice, we performed immunohistochemistry for single-stranded DNA (ssDNA), a detection marker for apoptosis-associated DNA damage. We detected ssDNA-positive cells (apoptotic cells) in the retinal ganglion cell layer and outer nuclear layer of the peripheral retina in Del605–607 mice (Fig. 4B, arrows). In the retinal flat mount, apoptotic RGCs were also observed in the peripheral region of Del605–607 mice (Fig. 4B).

Evaluation of Wt and Del605–607 primary RGC axon out growth

To evaluate the axon outgrowth of RGCs for Del605–607 mice, we first developed a double transgenic mouse by mating Del605–607 mice with Thy1 promoter-driven cyan fluorescence protein (Thy1-CFP) transgenic mouse, which enables visualization of RGC with CFP filter. Primary RGC culture of Del605–607/Thy1-CFP double transgenic mice was successfully established and the axon growth was monitored photographically (Fig. 5A). The RGC axon out growth rate of Del605–607/Thy1-CFP transgenic mice was reduced by ~60% compared with those from Thy1-CFP mice alone

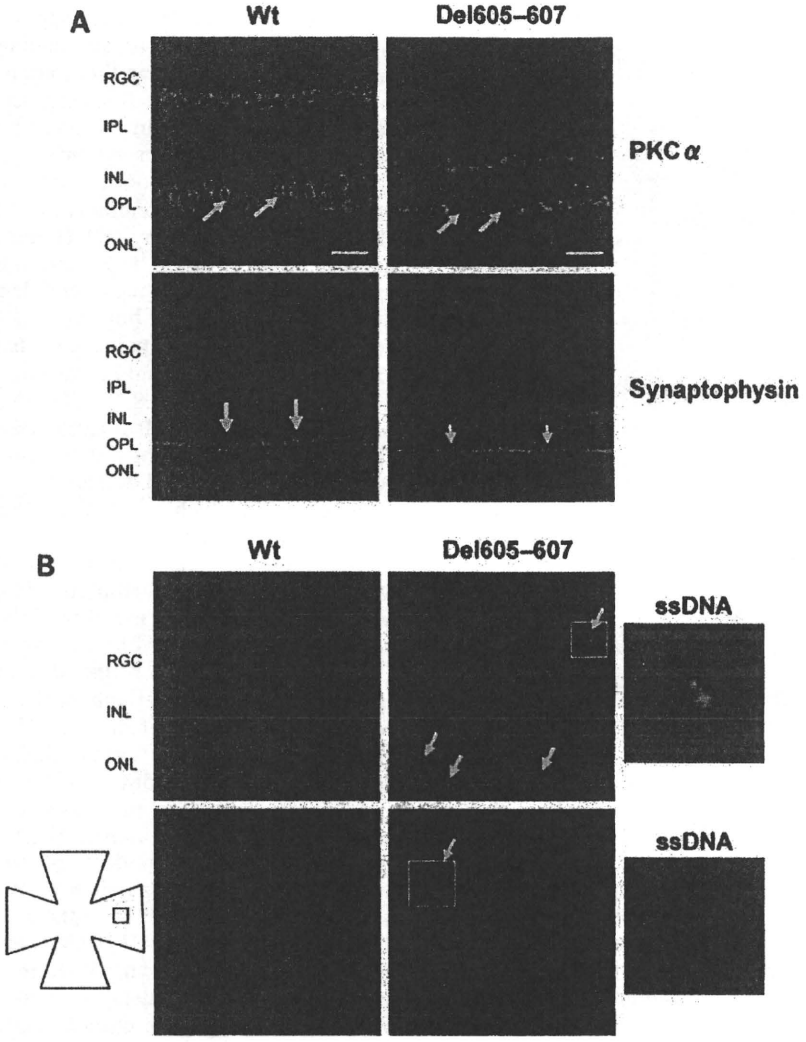

Figure 4. Degeneration of outer plexiform layer (OPL) and outer nuclear layer at the peripheral retina of Del605–607 mouse. (**A**) Immunostaining of the retina sections with tyrosine hydroxylase (red) and PKC α (green), a specific maker for dopaminergic amacrine cells and rod bipolar cells, respectively (upper panel). Cell loss and size reduction of bipolar cells was observed. Scale bar, 20 μm. Immunostaining of the retina sections with synaptophysin, a specific marker for neuronal presynaptic vesicles (lower panel). Synapse disruption (arrow) was observed in the OPL of Del605–607 mouse peripheral retina. Scale bar, 50 μm. (**B**) Immunostaining of cryosection and flat mount retina with specific apoptosis marker, ssDNA. Apoptosis cells were observed in the all cell layers in the peripheral retina of Del605–607 mice. Scale bar, 50 μm.

at the fifth day of culture. This finding demonstrated that the Del605–607 mutation can directly influence the RGC axon outgrowth *in vivo*.

Molecular modeling of mouse Wdr36

In order to model a three-dimensional structure of mouse Wdr36, we thread a sequence of Wt Wdr36 through the database of known protein structures using the SMART 6 engine (13). The engine recognized eight WD-40 β-propeller repeats, each repeat a motif of 40 amino acid residues often terminating in Trp-Asp (W-D) dipeptide. The *E*-value was changed from 1.46E−01 to 1.43E+1 for these repeats. The most significant change was observed for the motif at 559–598 with an *E*-value of 2.2E−10. Modeling by PHYRE (14) suggests that a structure of mouse Wdr36 is homologous to yeast actin interacting protein 1 (PDB-file: 1nr0) as the best hit between 14 different protein structures with a very low PHYRE *E*-value. This structure is likely to fold in two 7-bladed β-propeller domains (total 14 WD-40 repeats) forming a circularized structure in positions from 1 through 642 of the mouse Wdr36 sequence. The rest of the amino acid sequence (residues 646–899) show similarity to the large fragment of Utp21 domain of unknown structure that starts at position 668 and ends at position 896 with the SMART *E*-value for the domain of 2.40E−39. This result confirmed that Wdr36 and yeast Utp21 are structurally similar and share two 7-bladed β-propeller domains as a common structural motif (10,11).

Further, the structural features of the Wdr36 are similar to that of *Caenorhabditis elegans* UNC-78/AIP1 described

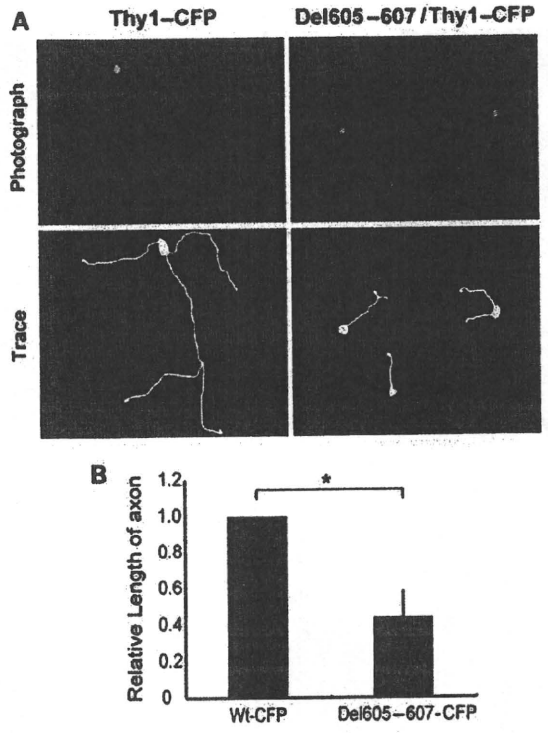

Figure 5. Reduced axonal extension in primary cultured RGCs by Del605–607 mutation. (A) Primary cultured RGCs of Wt and Del605–607 mouse (upper panel). Trance of axonal extension are shown in lower panel. Shorted axons were observed. (B) Quantification of the related axon length with Image J software.

earlier (15). The WDR structure revealed two distinct domains (Fig. 6A). The individual domain is a seven-bladed β-propeller exhibiting a significant structural similarity (Fig. 6B). Each blade is arranged into four anti-parallel β-strands labeled from A to D starting from the center of the propeller. Each blade is stabilized by hydrogen bonds between main chain atoms of β-strands as exhibited in Figure 6C for blades 6 and 7 that were targeted by site-directed mutagenesis in this work. Interaction between D and C β-strands in blade 6 is supported by four main chain–main chain hydrogen bonds, including Ile605O–Thr596N (2.8 Å), Ile605N–Thr 596O (3.0 Å), Cys607O–Val594N (3.3 Å) and Cys607N–Val594O (2.8 Å), and by one side chain–side chain hydrogen bond Asp606OD2–Arg595NH1 (1.8 Å). The circular shape of Wdr36 is maintained by the closure mechanism similar to that of a seven-bladed β-propeller in which the immediate amino-terminus serves as an outer β-strand (D) for the blade 7 (15,16) and by hydrophobic interactions located at the surface of blade 7 residues Val617, Met619, Val631, Leu634, Ile636 and Leu638 (Fig. 6C) and at the surface of the blade 1 residues Leu329, Ile332, Tyr334, Ile342 and Phe361 (not shown).

DISCUSSION

In this study, phenotypic features of mice overexpressing mutant *Wdr36* were determined and characterization of RGC was performed *in vitro* and *in vivo*. Molecular modeling techniques were additionally applied to simulate mouse Wdr36 protein structure for calculating the structural change induced by three mutations that were introduced in transgenic mouse models. This is the first demonstration of an association between gene mutations in *Wdr36* and changes in a phenotype observed in a mammalian system.

The design of the D606G transgene construct was based on the original paper by Monemi *et al.* (5). Our molecular modeling shows that mouse D606G mutant, equivalent to the human D658G mutation, is located in the seventh β-propeller of the second domain. This seventh β-propeller of the second domain is conserved for both amino acid sequence and molecular structure. Previous studies have predicted that the D658G variant was strongly associated with severe phenotype in glaucoma patients (5,8,11). To elucidate molecular functions in this region, we also developed a 3 amino acid deletion (Del605–607) containing D606 position at the seventh β-propeller of the second domain and a 40 amino acid deletion (Del 601–640), which deletes the entire seventh β-propeller of the second domain.

Two previous functional studies have demonstrated that WDR36 is involved in ribosome biogenesis similar to the yeast Utp21, which is a member of the small subunit processome complex responsible for maturation of 18S rRNA (10,11). Footz *et al.* has further demonstrated that expressing the equivalent human variants in Utp21 can cause significant reduction or elevation of the pre-rRNA level in the nucleoli. Among the 11 variants tested, Utp21 D621G equivalent to the human WDR36 D658G gave the lowest pre-rRNA level in yeast and the highest pre-rRNA level by 216% in the Sti1 null yeast strain (11). In human, all genomic sequence variants exclusive to glaucoma patients or variants with low or high incidence in control population did not correlate with functional studies in yeast. The authors of this paper concluded that human R529Q, I604V, D658G and M671V are likely to encode subtle defects in WDR36 that in concert with another susceptible gene(s) or with certain environmental factor(s) may trigger the onset of POAG.

These data suggest that in human WDR36 the D658G variant may be functionally the most influential mutation and contribute to the onset of the disease as the genetic modifier. In fact, WDR36 has been previously suggested to influence the severity of MYOC-based POAG (6). To verify the above-mentioned hypothesis, further investigation would be necessary. Such investigation is in progress by cross-mating Del605–607 mice with other glaucoma mice, such as the myocilin Y423H transgenic developed by Zhou *et al.* (17) to validate the POAG-like phenotype with RGC loss and increased IOP.

In spite of the fact that mutant Wdr36 was expressed in all tissues, it is surprising that defects were only observed in the retina. Previous studies by Skarie and Link (10) have shown loss of wdr36 function in zebrafish resulted in developmental defects including liver necrosis and absence of swim bladder inflation by 6 days post fertilization. Small head and eye was also reported with lens opacity and thickening of lens epithelium but relatively mild defect in the retina even after 6 months post fertilization. In contrast to zebrafish, transgenic mice with ubiquitous expression of the mutant Del605–607 revealed a progressive defect in the retina but not elsewhere including the anterior part of the eye even 16 months after

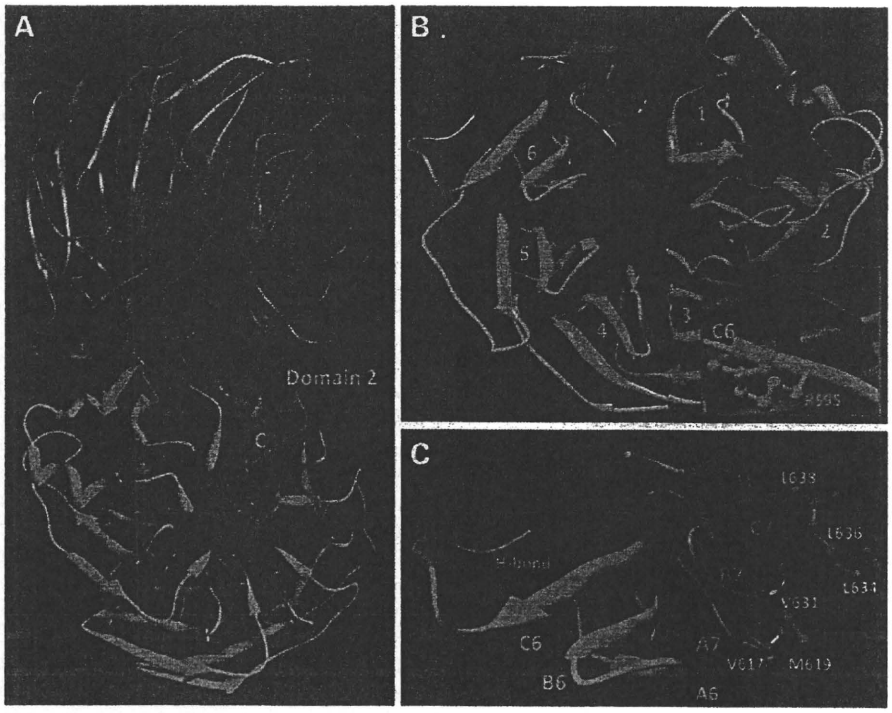

Figure 6. The WDR36 three-dimensional structure is obtained by homology modeling. The ribbon model with β-strands shown by arrows illustrates a proposed structure of WDR36 containing 14 WD40 repeats. N- and C-terminal domains with a seven-bladed β-propeller fold are shown by orange and cyan, respectively (**A**). In domain 2, individual blades with the WD40 structural motif are numbered from 1 to 7 (**B**). Similar to others, blade 6 is composed of an antiparallel β-sheet with the individual β-strands labeled from A6 to D6 (**C**). The individual β-strand D6 and the seventh blade of the domain 2 which correspond to mutations Del605–607 and Del601–640 are shown by blue and green, respectively. The Wt amino acid side chains that are important for the analysis of sequence variants are shown by ball and stick models. Hydrogen bonds are shown by cyan and orange lines. Interaction between residues R595 and D606 is revealed as an inset in (B). The missense mutation D606G cause the D606 side chain removal and breaks the single side chain–side chain hydrogen bond Asp606OD2–Arg595NH1. Amino acids are shown by a single letter code.

birth. In gross anatomical examination, the size and structural abnormalities of head, eye and gut, which occurred in zebrafish, were not observed in mice. The vulnerability of the retina in the mouse model may suggest a differential role of Wdr36 in the two species, perhaps through interaction with different retina-specific molecules. On the other hand, Skarie and Link (10) also showed the involvement of the p53 pathway and subsequent activation of p21 on the effects of the loss of Wdr36, suggesting that the p53 pathway may also have influenced the phenotype of our transgenic mice.

Overall, the adult Wdr36 transgenic mice with abnormal phenotype serve as the potential POAG model for future use. To date, a number of animal models for glaucoma have been established (12,18–24). Interestingly, the phenotypes of human glaucoma mutation-based mouse models including myocilin Y423H (20,17), optineurin E50K (12) and Wdr36 Del605-607 (Figs 2–4) all involve loss of peripheral RGCs accompanied by peripheral retinal degeneration. Herein, we raise the question, what are the reasons for peripheral retinal degeneration? Previous reports have indicated that mouse models of glaucoma follow similar natural courses of peripheral retinal degeneration (12,17–20). These findings suggest that all three mouse models share a common signaling pathway for RGC death and beyond, although the function of each protein is distinct. Wdr36 transgenic mouse will be useful in combination with other models to identify molecules responsible for this common pathway of RGC death.

Prediction by homology structure of Wdr36 was used to analyze three mutant variants D606G, Del605–607 and Del601–640, respectively (Fig. 1A). The missense change of aspartic acid to glycine at position 606 interrupts the side chain–side chain hydrogen bond Asp606OD2–Arg595NH1 without affecting other hydrogen bonds that stabilize interaction between C6 and D6 β-strands (Fig. 6B, inset). This minor change suggests that the mutation will show either no effect or an insignificant structural change in the stability of the protein with age that could potentially appear at a very slow rate. In contrast, the mutation Del605–607 removes residues from positions 605 to 607 corresponding to the β-strand D6 (Fig. 6A–C, blue). This results in interruption of five hydrogen bonds in Wdr36 structure, and might affect the stability of the 6th blade of domain 2 (Fig. 6B). Although it is difficult to make a definite conclusion, our modeling predicts that the polypeptide chain might still adopt a β-propeller conformation. Thus, domain 2 will continue to adopt a seven-blade β-propeller structure, suggesting that protein–protein interactions that involve residues after position 607 might be significantly perturbed because all interacting residues will be shifted by three residues from their original positions. Further, this could exclude the mutant variant from the